Empirical validation and local sensitivity analysis of a lumped-parameter thermal model of an outdoor test cell

G. Cattarin[1,2,3,*], L. Pagliano[1], F. Causone[1], A. Kindinis[2,3], F. Goia[4], S.Carlucci[5], C. Schlemminger[6]

[1] end-use Efficiency Research Group, Department of Energy, Politecnico di Milano, Milano, Italy

[2] Université Paris-Est, Institut de Recherche en Constructibilité, ESTP, Cachan, France

[3] Efficacity, Marne la Vallée Cedex 2, France

[4] Department of Architecture and Technology, Faculty of Architecture and Design, Norwegian University of Science and Technology, NTNU, Trondheim, Norway

[5] Department of Civil and Environmental Engineering, Faculty of Engineering, Norwegian University of Science and Technology, NTNU, Trondheim, Norway.

[6] SINTEF Building and Infrastructure, Department of Architecture, Materials and Structures, Trondheim, Norway.

[*]Corresponding author: giulio.cattarin@polimi.it

Abstract

This paper presents the experimental validation of a thermal model describing the ZEB Test Cells Laboratory, located at the Gløshaugen campus of NTNU and SINTEF in Trondheim, Norway. Besides, a local sensitivity analysis identifies the parameters and inputs that are most influential on the thermal behaviour of the test cell, in terms of temperature profiles of the internal air and internal surfaces. The analysis shows that, in free-running conditions, the most important parameters and inputs, out of the 49 tested ones, are: the air temperature in the guard zone, the initial temperature(s) of the test cell envelope, the linear dimension of the square window, the solar irradiance on the vertical plane of the window, the depth of the test cell, the thermal conductivity and the thickness of the polyurethane layer in the envelope, the solar direct transmittance of the window, the internal height and width of the test cell, the external air temperature and the electrical power input to the mixing fan. Based on the outcome of the local sensitivity analysis and on in-field observations, some practical measures to improve the quality of the input data provided to a dynamic energy simulation tool, and thus the accuracy of prediction of the temperature evolution of the test cell. For example, we suggest monitoring accurately the environmental conditions in the guard zone, which are particularly influential under free-running conditions, and installing a global irradiance pyranometer next to the window in order to reduce the uncertainty related to the entering solar load.

Keywords: guarded test cell; experimental validation; sensitivity analysis; measurement techniques; Matlab

1. Introduction

The goal of the present study is to identify actions that can improve the measurement techniques adopted in outdoor test cell experiments. This has been achieved by (i) modelling the thermal behaviour of an existing test cell adopting a lumped-parameter approach, (ii) comparing the obtained simulation results with measurements, (iii) performing a local sensitivity analysis in order to highlight the most relevant model inputs and parameters.

The influence of a model parameter depends also on the specific experimental conditions and on the algorithms used by the thermal model. Thermal simulations and sensitivity analyses applied to a range of expected operating conditions can guide the design process of new test cell facilities and the operational procedures in new and existing ones. Highlighting the most critical parameters can support the research team in the choice of the features of the envelope, of the conditioning system and of the measurement set-up and in the choice and control of conditions under which specific experiments are performed.

1.1. Lumped-parameter thermal models for building energy simulation

In general terms, the lumped-parameter approach (also called thermal-network approach) consists of discretizing the temperature field of a thermodynamic system, by identifying a certain number of representative nodes where an energy balance is computed. Each node is connected to the adjacent nodes by means of thermal resistances, and thermal capacities are assigned to all elements that are capable of storing internal energy, such as walls, transparent elements (whose thermal capacity is in some cases assumed negligible), water tanks, and relevant volumes of air (e.g., the whole air volume inside a room or a whole building, while usually the thermal capacity of the air volume in the gap of double-glazing unit is considered negligible). Thermal bridges are usually treated in a simplified way, for example by decreasing the thermal resistance of adjacent elements by an estimated quantity. Common underpinning hypotheses when adopting a lumped-parameter thermal model are that (i) each node represents a sufficiently small finite volume (i.e., a portion of a solid body or a liquid/gas volume) to be considered at uniform temperature; (ii) air is perfectly

transparent to electro-magnetic radiation, hence not involved in radiative heat exchanges, (iii) thermal capacities and thermal conductivities are time-invariant and independent from temperature and moisture content; (iv) convective and radiative heat transfer coefficients are constant within the calculation time step. The hypotheses at points (iii) and (iv) are necessary to consider the thermal system as linear, hence permitting the superimposition of effects. Additional hypotheses that are specific to each model (and whose validity has to be evaluated for each individual model) concern the interactions between the elements: only main heat exchanges are considered, neglecting minor heat flows. Examples of often neglected heat flows are those due to local non-homogeneities in the construction elements.

Lumped-parameter models are also closely correlated to physical characteristics of the thermal system (hence being classifiable as *white box* models) and they allow for an intuitive graphical representation in the form of resistor–capacitor (RC) circuits. In the following paragraphs, we propose a selection of previous studies dealing with specific aspects of linear lumped-parameter thermal models. For a theoretical background, the reader can also refer to Athienitis and Santamouris [1], Davies [2] and Underwood and Yik [3].

Hudson and Underwood [4] propose a simple building model coupled to the model of a convective heat emitter for the purpose of investigating control system design. The lumped-parameter model proposed by the authors worked well for short-term dynamics, but began to diverge from experimental data on the long-term (> 45 h). The study compares the results obtained with first-order and second-order models of the external walls and the ceiling (in the latter case two thermal capacitances were assigned to those building components). The authors conclude that, on a short-term horizon, no appreciable advantages can be observed with the higher-order model when predicting the internal air temperature. However, the study does not investigate the temperature evolution across the envelope; in fact, physical considerations suggest that only a fraction of the thermal capacity of the building is activated by phenomena such as solar radiation or internal gains. Depending on the thermal characteristics of the building envelope and the fluctuations of the boundary conditions, a variable fraction of the *apparent thermal capacitance* (which results by adding the distributed thermal capacities of all building elements into a lumped capacitance, as stated in Antonopoulos and Koronaki [5]) may be activated. This means that only a portion of the envelope may show temperature changes within the investigated time span and hence vary its internal energy. Antonopoulos and Koronaki [5]

state that «The real or effective thermal capacitance of buildings, which quantifies the ability of a building to store thermal energy and is useful in dynamic thermal performance calculations, differs considerably from the apparent thermal capacitance, as the ability of structural elements and furnishings to store heat is different when these are distributed in the building or considered together forming a unified volume».

The determination of this effective thermal capacitance is however a complex task, which shall take into account both the characteristics of the building envelope and the variation of the boundary conditions. In a study investigating strategies for minimizing the peak cooling demand by thermally activating the building structures, Lee and Braun [6] conclude that the effective thermal capacitance «would probably be somewhere between the internal and total building capacitance values, but closer to the internal capacitance», meaning the capacitance of the internal air, the furnishing and the internal walls.

The works by Gouda et al. [7] and by Fraisse et al. [8] investigate more in depth the impact of the model order on the accuracy of the results, where the model order reflects the number of thermal capacities assigned to each building element.

A more recent work by Underwood [9] proposes an improved method for the extraction of simplified model parameters based on a multiple-objective-function search algorithm and the use of a reference model based on a rigorous finite-difference method. In particular, Underwood develops an optimization procedure to adjust the resistance and capacity distributions of a second-order model in order to enable a correct prediction of the surface temperatures.

In summary, despite the abundant presence of more complex models, the lumped-parameter thermal models are still currently used (i) in fit-for-purpose manner (e.g. when it is necessary to develop a simple white box model of a physical phenomenon) (ii) because, if properly constructed, they can describe a physical phenomenon with a good accuracy, and (iii) since they are very effective computationally-wise.

1.2. Empirical validation of building energy models

The US Department of Energy's Advanced Simulation and Computing (ASC) program defines *validation*, as «the process of confirming that the predictions of a code adequately represent measured physical phenomena». As highlighted by Trucano et al. [10], validation differs considerably from *verification* and *calibration*, where the former aims at assessing the mathematical accuracy of the numerical solutions; while the latter is a process in which a certain set of parameter values are fine tuned to improve the agreement

between the numerical predictions and the chosen benchmarks. In particular, the authors underline that the calibration should not be used to increase the credibility of a certain calculation code.

In the present work, the main objective is to improve the quality of the match (in other terms, the range and appearance of residuals) only by physical considerations; the model parameters are kept at their *nominal values* (e.g., the values provided by the technical sheets of the building materials). Therefore, we here adopt the conclusions by Trucano et al. [10] and we exclude the calibration phase from the present validation process. For a deeper discussion on the topic of validation of building energy simulation models the reader can refer to the works by Judkoff et al. [11], Judkoff et al. [12] and Cattarin et al. [13]. In addition, the literature review by Cattarin et al. [14] presents an overview of experimental studies that used outdoor test cell facilities to validate airflow and daylight models and to characterize the performance of single building components or control systems. The review reports and discusses also the potential sources of discrepancy between measurements and numerical predictions.

1.3. Brief introduction to sensitivity analysis

Sensitivity analysis has been defined as «the study of how uncertainty in the output of a model (numerical or otherwise) can be apportioned to different sources of uncertainty in the model input» [15]. An intuitive definition is given by Lam & Hui [16]: «In the simplest terms, the aim of sensitivity analysis is to compare quantitatively the changes in output with the changes in input». The final goal is to guide research priorities towards factors that are responsible of the greatest output variability, with the design aim of achieving energy savings, improvement of comfort conditions and others ([16], [17]). Sensitivity analysis is strictly related to uncertainty analysis: while the former determines and ranks the most important set of parameters affecting a given model output, the latter quantifies the variation of the model output given the uncertainty ranges of the model inputs [18]. For example, Pagliano et al. [19] report an uncertainty analysis applied to the measurement of the solar factor under dynamic conditions, for alternative configurations of outdoor test cell facilities.

In recent years, the number of scientific publications developing and/or adopting sensitivity analysis techniques has rapidly increased, also thanks to the huge increase of computational power, which allows for a large number of simulations to be implemented. The applications of sensitivity analysis to building energy

simulation are numerous, such as (i) investigating alternative design options in case of new buildings, (ii) selecting the renovation measures with the highest energy-saving potential for retrofit of existing buildings, and (iii) detecting the most likely sources of discrepancy between measurements and predictions [20]. Concerning the calibration of thermal models, sensitivity analysis may be used to reduce the number of free variables of a model [21] by identifying *insensitive parameters* (parameters that do not have a significant impact on the simulation results) and setting them at their nominal value, i.e., excluding them from the parameter calibration. A relatively recent field of application of sensitivity analysis is represented by robustness studies that investigate the impact of design strategies on energy consumption and comfort levels for various climate-change scenarios [22].

In the literature, several classification schemes have been applied to sensitivity analysis methods [1-4]. In the present work we refer to the one proposed by Heiselberg et al. [23], who classify sensitivity analysis methods as screening, local and global methods. Screening methods and local sensitivity analysis (LSA) methods rely on an One-parameter-At-a-Time (OAT) methodology, by which the modeller evaluates the impact on the results of the variation of a single parameter while all other input parameters are held constant at their reference value [24]. Both screening and LSA methods are carried out in a deterministic framework, precluding the assignment of a probability distribution to the model inputs [25]. In other terms, all parameter values are considered equally probable within a specified range (uniform-probability distribution). In addition, these methods do not treat correlations among parameters or any non-linear and non-additive model behaviour [24]. Despite those limits, LSA methods are still largely used in building simulation (e.g., [26], [27] and [28]) due to their advantages in terms of low computational cost, simple implementation, and easy interpretation [20]. Screening methods are more specifically used to reduce large sets of parameters to smaller sets before applying global sensitivity analysis methods, which are more computationally demanding ([24], [29]). In the simple case of «a time invariant linear system, whose input time series boundary condition experiences a time continuous invariant perturbation» [21], the first-order sensitivity functions are expressed by the partial derivative of the output *y* with respect to each of the input parameter $x_i\big|_{i=1}^{n}$. In the case of building energy simulations tools, the relationship between the outputs and the inputs may be strongly non-linear and input parameters may be correlated to each other. In general terms, for OAT

methods, given n parameters, the gradient of the output $f(\mathbf{x}) : \mathbf{x} \in \{x_1 , x_2 , \dots , x_n\}$ with respect to the parameter chosen for the analysis –let's say x_1– will be:

$$\frac{df(\mathbf{x})}{dx_1} = \frac{\partial f(\mathbf{x})}{\partial x_1} + \frac{\partial f(\mathbf{x})}{\partial x_2} \times \frac{dx_2}{dx_1} + \frac{\partial f(\mathbf{x})}{\partial x_3} \times \frac{dx_3}{dx_1} + \dots + \frac{\partial f(\mathbf{x})}{\partial x_n} \times \frac{dx_n}{dx_1} \quad (1)$$

When the inputs are independent, that is when $dx_2 / dx_1 = dx_3 / dx_1 = \dots = dx_n / dx_1 \neq 0$, the total derivative is equal to the partial derivative of the output $f(\mathbf{x})$ with respect to the chosen parameter x_1.

In order to take into account the probability distribution of input parameters and their interactions, Global Sensitivity Analysis (GSA) methods are also available. They are classified by Tian [20] according to four approaches: regression, screen (e.g., the Morris method), variance-based (e.g., the Sobol method) and meta-model methods. While LSA focuses on the effects of uncertain inputs around a point (or base case), GSA can explore the whole input space. In addition, most GSA methods allow for self-verification, that is they provide the proportion of variance of the model output which is explained by the investigated input factors [20]. While LSA methods vary one parameter at a time, in GSA an input vector/matrix is generated by means of an appropriate sampling method, with parameters values sampled from their probability density functions [23]. For in-depth information on the subject of GSA methods, the reader can refer to the reviews by Tian [20] and by Borgonovo and Plischke [25]. An interesting study by Kristensen and Petersen [24] investigates how (i) the choice of the sensitivity analysis technique and (ii) the level of *a-priori* information on the probability distribution of the parameters can affect the identification and ranking of input parameters. The study shows that the LSA method seems appropriate to identify the set of most significant parameters, but should not be used for a final assessment of the relative importance of one parameter with respect to others that are close in the ranking.

The selection of the sensitivity method cannot disregard the computational effort: Kristensen and Petersen [24] report that the number of model evaluations was 49 for the LSA, 6250 for the Morris method and 260 000 for the Sobol method. According to Sanchez et al. [30], a variance-based analysis for a 12-input parameter model requires about one hundred times the computational cost of a first-order Morris analysis.

When feasible, the most rigorous approach may be that of applying two or more sensitivity analysis methods to increase confidence in the results, as proposed by Tian and de Wilde [22] and Yang et al. [31].

The following Sections present an experimental validation of a lumped-parameter thermal model of a test cell based on a dedicated experimental campaign at the Zero Emission Buildings (ZEB) Test Cells Laboratory, located in the Gløshaugen campus of the Norwegian University of Science and Technology (NTNU) and SINTEF in Trondheim, Norway. The paper shows that the validation of a model, although useful to evaluate the quality of the simulation results, does not produce information to improve the management or guide the design of future experimental facilities. Nevertheless, if coupled with a sensitivity analysis, it may become a fundamental guidance for the scholar running experiments, for the facility operational manager, and for companies, research centres, and university interested in developing new experimental facilities. The local sensitivity analysis performed and presented in this work, indeed allowed us to highlight the model parameters and inputs that are most *sensitive*, that is the ones that have a high impact on the outputs of interest (e.g., the temperatures of various elements of the test cell). The results of the sensitivity analysis and of in-field observations provide insights on actions that may improve the quality of the input data provided to a computer-aided simulation tool, and hence improve the fidelity of the predicted thermal behaviour of the test cell. They provide also important information for an optimized operation of the facility and, to a certain extent, for the design of similar new ones.

2. Description of the facility and experimental protocol

The ZEB Test Cells Laboratory building is located at the Gløshaugen campus area of NTNU and SINTEF (63°41' N; 10°41' E, altitude: about 40 m a.s.l.) and hosts two independent cells exposed to south (azimuth of the exposed surface: +5° towards west). The facility (Figure 1) is designed to host building envelope components and building equipment components (e.g., air distributions systems and heating/cooling terminal units) in order to study their energy performance and their impact on the indoor environmental quality. Each test cell is surrounded by a dedicated guard zone, thus allowing for «parallel tests of the same building envelope technology/equipment with different indoor air temperature set-points, occupancy schedules or operations», as reported by Causone et al. [32]. Hence, the facility can be classified, following the criteria proposed by Cattarin et al. [14], as *comparative and absolute-guarded*, since it is conceived to (i)

simultaneously expose to the same external environment two building components installed on the south façade (comparative approach) and/or (ii) carry out performance assessments by means of a calorimetric measurement in each cell (performance expressed in absolute terms, in a guarded cell).

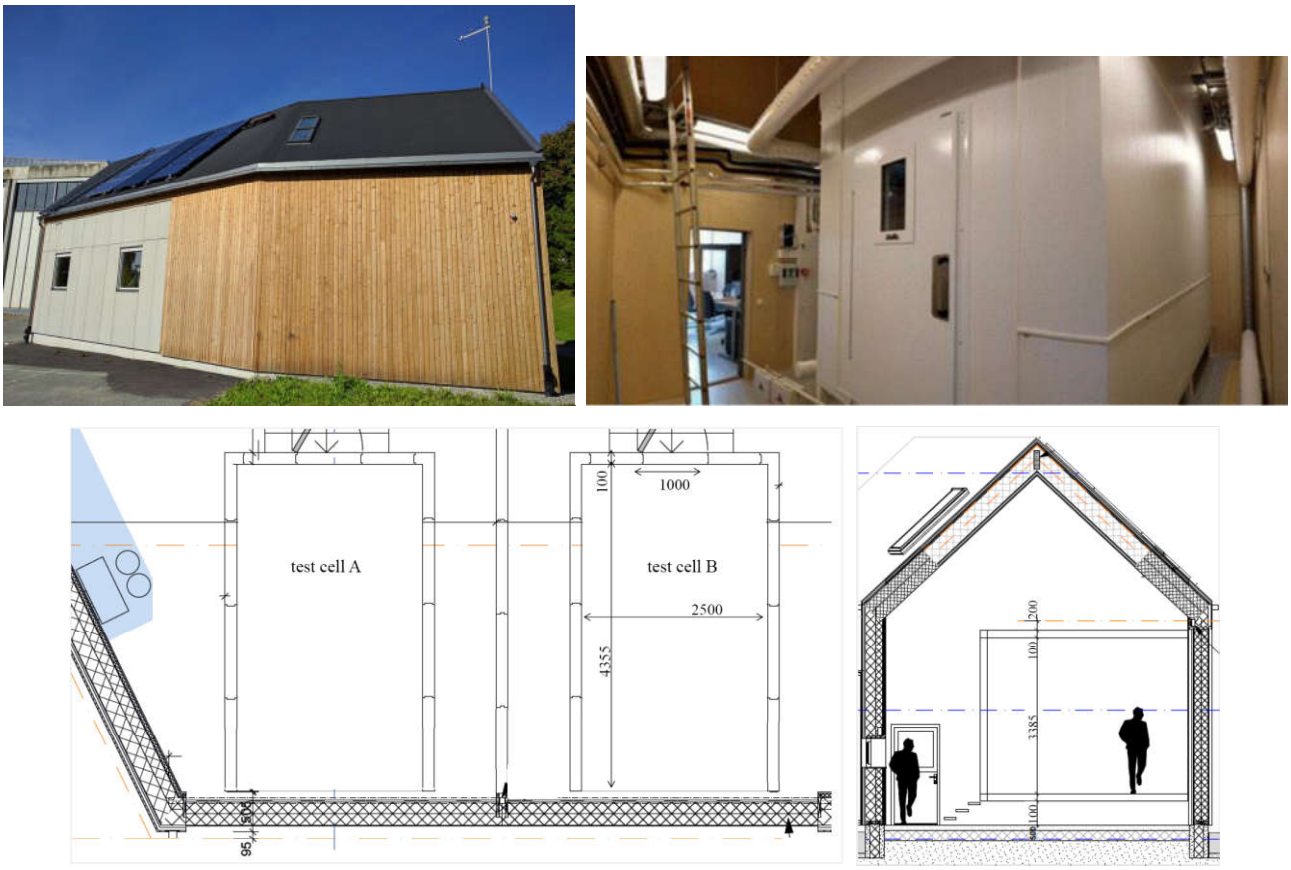

Figure 1. On top: external view (left) and internal view (right) of the ZEB Test Cells Laboratory. The grey façade hosting the two windows corresponds to the external façades of the two test cells. The mast on the roof (top right) holds the pyranometers measuring the global horizontal radiation and the global radiation on a south-exposed plane. On bottom: plan view (left) and vertical section (right) of the ZEB Test Cells.

2.1. Opaque and transparent envelope components

Each test cell has internal dimensions of about: 4.36 m x 2.50 m x 3.39 m, respectively width, depth and height, with five envelope elements (including the floor and the ceiling slabs) in contact with a dedicated guard zone, while the external south wall hosts the window. The air supply system in the guard zone achieves a uniform air-temperature distribution all around the test cell. The layers constituting the envelope elements of the test cell are described in Table 1 and Table 2. The elements facing the guard zone (north, east and west walls, floor slab and ceiling slab) are sandwich panels insulated by means of 10 cm of polyurethane foam (thermal transmittance U_{env} = 0.21 $Wm^{-2}K^{-1}$), while the external wall (exposed to south) has a higher level of insulation in order to cope with higher temperature differences (U_{south} = 0.11 $Wm^{-2}K^{-1}$). The external

wall can be adapted, depending on the experimental needs and the tested technology. The test cell can be accessed via an insulated door (sandwich panel with 8-cm polyurethane between two galvanized-steel sheets, $U_{door} = 0.29\ Wm^{-2}K^{-1}$). While the design of the envelope derives from industrial know-how on cold chambers, additional precautions have been taken in order to minimize air infiltrations. The most critical points of the test cell (the entrance door, the through holes in the envelope for the passage of electrical cables, ventilation ducts and the interfaces between the window and the south wall and between the latter and the test cell envelope) have been sealed by means of silicone and tape. The internal surfaces of the walls are realized with white paint on steel substrate, hence it is estimated that the surface absorptance is about 0.3 and the surface emissivity is about 0.9.

Table 1. Construction of the walls, the ceiling slab and the floor slab

Internal walls	Thickness (m)	Thermal conductivity ($W\ m^{-1}K^{-1}$)	Density ($kg\ m^{-3}$)	Specific heat ($J\ kg^{-1}\ K^{-1}$)
steel – galvanized sheet	0.0006	62	7800	500
polyurethane foam	0.0988	0.024	35	1600
steel – galvanized sheet	0.0006	62	7800	500
internal wooden flooring (only floor)	0.15	0.15	1250	1200

Table 2. Construction of the south wall (in contact with the exterior)

South wall	Thickness (m)	Thermal conductivity ($W\ m^{-1}K^{-1}$)	Thermal resistance ($m^2K\ W^{-1}$)	Density ($kg\ m^{-3}$)	Specific heat ($J\ kg^{-1}K^{-1}$)
external cladding	0.005	0.5	0.01	1250	1200
air cavity*	0.02	*n.a.*	0.18**	1.2	1007
glass-wool layer***	0.30	0.035	8.57	32	670
internal wooden lining	0.012	0.15	0.8	1250	1200

n.a. stays for not applicable, * air cavity and glass-wool layer are separated by an air barrier
** estimated from EN ISO 6946 : 2007 – Building components and building elements – Thermal resistance and thermal transmittance -Calculation method
***two 0.15 m thick layers separated by an air barrier in the middle

The window installed on the south wall consists of an argon-filled (90%) triple glazing (4/12/4/12/4) of dimensions: 1076 mm x 1076 mm, with two low-emissivity coatings and a PVC frame. The thermal and/or optical properties of the single pane, the glazing unit and the entire window according to the manufacturer are reported in Table 3. The window's thermal transmittance includes the thermal bridge between glass panes, the dividers and frame. The test cell faces a parking lot with concrete pavement and a green grass lawn. Some trees at about 15 m distance cast a shadow on the test façade in the first part of the morning in summer months.

Table 3. Thermal and optical properties of the single pane, the glazing unit and the window

Glazing unit			Single panes	Window
Solar direct transmittance (τ_{12})	Solar direct absorptance (α_{Tot})	Solar direct reflectance (ρ_{12})	Solar direct absorptances (α_{int} ; α_{mid} ; α_{ext})	Thermal transmittance (U_w, in W $m^{-2}K^{-1}$)
0.33	0.19	0.48	0.12 ; 0.03 ; 0.04	0.7

2.2. Measurement set-up and experimental procedure

The test cell is fully instrumented in order to monitor the temperatures of the envelope surfaces and the internal air. The internal gains due to the mixing fan and the active sensors (Pt100 resistance thermometers) are measured by a wattmeter. The temperatures of the internal and external surfaces of the envelope are measured by means of T-type thermocouples, with accuracy of ± 0.4 °C. Each external surface facing the guard zone is monitored by six thermocouples, evenly distributed over the surface and averaged before logging. The air temperature of the guard zone is measured by six sensors (thermocouples) placed 5 cm from the walls of the test cell, giving an average air temperature for each side. The sensors measuring the internal air temperature (Pt 100 RTD) are installed at three heights (0.1 m, 1.6 m and 2.6 m) in the centre of the test cell in order to detect possible air temperature stratifications. The external weather parameters are measured over the roof of the facility at a height of about 10 m (Figure 1, top right); their accuracy levels are reported in Table 4. Three pyranometers measure the global solar irradiance on the horizontal and vertical planes and on a plane tilted at 42° (this last one is used for analyses of the roof-mounted PV panels and solar thermal panels).

Table 4. Characteristics of the sensors for the measurement of weather conditions. "% m.v." stands for "percentage of measured value"

Physical variable	Type of sensor	Accuracy
external air temperature	Pt100 1/3 DIN RTD	± 0.15 °C ± 0.1% m.v.
relative humidity	capacitive	± 1.5%
wind speed and direction (10 m height)	ultrasounds	± 0.2 ms^{-1} ; ± 2°
global irradiance (measured on 3 planes)	pyranometers	2^{nd} class pyranometer

Measurements were taken from 8:00 A.M. of 9^{th} to 4:30 A.M. of 14^{th} September 2016; during this period the test cell was in free-running mode (no active cooling or heating). We shut and sealed the inlet and outlet air terminal units in the test cell in order to avoid possible infiltrations from the ventilation system. During the test we used a mixing fan, with an electrical power input approximately constant at 30 W, to reduce air temperature stratifications. Free-running conditions and a clear sky are of particular interest in the validation process, since the test cell experiences relatively large temperature swings due to the entering solar load (and

secondarily due to external temperature variations) and hence the model is *stressed* to test its ability to predict the temperature variations in a wide range. As discussed by Mateus et al. [33] in previous validation studies, the free-running case is the most critical in terms of maximum residuals of the internal temperatures.

3. Thermal modelling

The lumped-parameter thermal model is briefly summarized as follows. The model represents internal air as a single thermal node, based on the good temperature uniformity achieved by the use of the mixing fans; air infiltrations can be neglected, when the test cell is operated in free-running, due to the low pressure difference between the test cell and the control volume, and the good airtightness level of the cell. In order to assess air leakage, parametric tests at different pressure difference values between the cells and the control volumes were performed using a dedicated device, consisting of a fan located in a metal duct and equipped with air pressure and air flow meters, as traditional blower door devices are generally not sensitive enough to capture the small leakages of a test cell. The air leakage value was found to be lower than 0.3 h^{-1} when the pressure difference between the cells and the control volumes where 10 Pa. Under normal free-running operations, the pressure difference between the cells and the control volumes is well below 10 Pa, resulting in air leakages in the order of 10^{-1} air change per hour (ACH). The electrical power used by the mixing fan is assigned as internal power generation to the node representing the internal air.

The north, east and west walls have all the same construction and are in contact with the guard zone, where the air temperature is approximately uniform. In the present model, these three walls are represented by a single ninth-order element (11R9C). The ceiling slab is modelled separately to take into account that it is never directly hit by entering beam solar radiation. The floor slab is also modelled separately since it has an internal wooden flooring. Figure 2 shows the thermal nodes used to model each component of the envelope. The red circles represent the nodes that also correspond to the physical location of the sensors, while the blue circles are additional nodes used in the model to refine the description of the heat propagation through the envelope. The layers that are closer to the internal surfaces, as well as the external surface of the South wall, are discretized more finely in order to better predict the thermal dynamics resulting from rapid fluctuations

of solar radiation (e.g., due to transient clouds), while the nodes in the central layers of the envelope are more spaced.

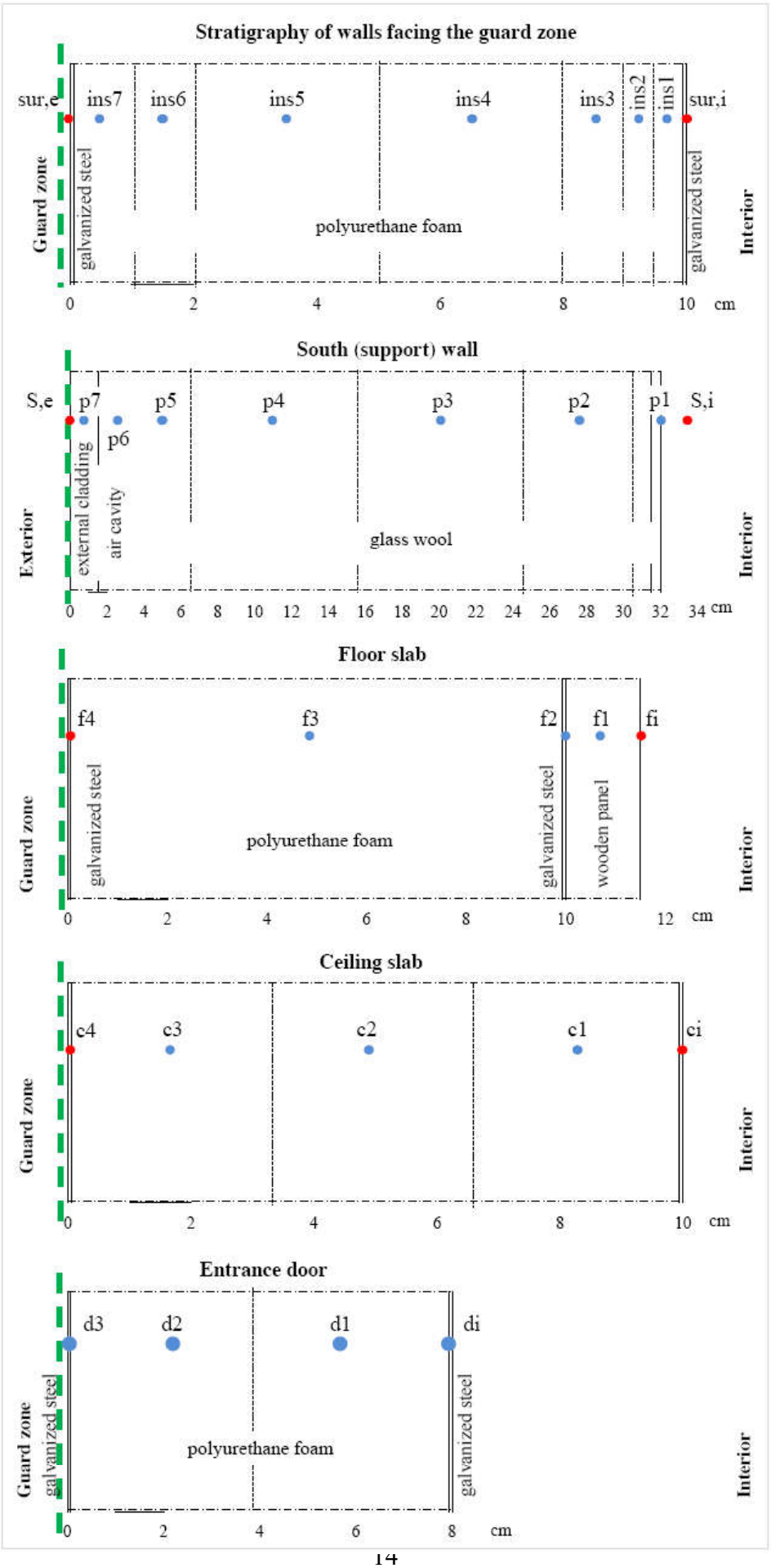
Stratigraphy of walls facing the guard zone
sur,e
ins7
ins6
ins5
ins4
ins3
ins2
ins1
sur,i
Guard zone
galvanized steel
polyurethane foam
galvanized steel
Interior
0
2
4
6
8
10
cm
South (support) wall
S,e
p7
p6
p5
p4
p3
p2
p1
S,i
Exterior
external cladding
air cavity
glass wool
Interior
0
2
4
6
8
10
12
14
16
18
20
22
24
26
28
30
32
34
cm
Floor slab
f4
f3
f2
f1
fi
Guard zone
galvanized steel
polyurethane foam
galvanized steel
wooden panel
Interior
0
2
4
6
8
10
12
cm
Ceiling slab
c4
c3
c2
c1
ci
Guard zone
Interior
0
2
4
6
8
10
cm
Entrance door
d3
d2
d1
di
Guard zone
galvanized steel
polyurethane foam
galvanized steel
Interior
0
2
4
6
8
cm

Figure 2. Thermal nodes assigned to the test cell's envelope. The red dots represent the nodes also corresponding to the physical location of the sensors, while the blue dots are additional nodes used in the model. The green dashed lines indicate the physical boundaries of the control volume chosen for the present simulation work.

The simulation is conducted using the nominal values of the materials' thermal properties and assuming thermal bridges equal to 41% of the envelope's transmission heat transfer coefficient, in accordance with the results of a finite-element numerical analysis in THERM carried out during the calibration phase of the facility [34].

Concerning the convective heat transfer coefficients between the internal surfaces and the internal air, we adopt the correlations given by Khalifa and Marshall [35] for vertical walls, floor and ceiling surfaces and valid for air-surface temperature differences lower than 5 °C. The simulation results show that, since the temperature difference between air and internal surfaces is small (due to the high level of insulation and airtightness and the operation of the mixing fan), these correlations provide values generally below 1.5 W/(m^{2}K). Similar values are obtained using the correlation proposed by Hatton & Awbi [36] for vertical surfaces. Regarding the long-wave heat exchanges, we adopt the so-called *zonal method* described by Rohsenow et al. [37].

The global irradiance $G_{g,South}$ measured by the south-facing pyranometer cannot be directly used for simulation purposes: in fact, as discussed in Section 4.3, the thermo-optical behaviour of the test sample is significantly different for the beam and the diffuse components of the solar radiation. Therefore, starting from measurement of the global irradiance on a horizontal plane, we calculate the beam component on the horizontal using the model by Reindl et al. [38], which is adopted also in the commercial software tool TRNSYS v.17 (Mode 2 of Type 69) [39]. Then, we project the beam component on the vertical plane of the test sample according to the geometrical considerations presented by Duffie and Beckman [40], obtaining $G_{beam,South}$. Finally, the total diffuse component (sum of the sky-diffused and the ground-reflected radiation) is derived as difference between $G_{g,South}$ and the beam component $G_{beam,South}$. Being non-directional, in the literature and in commercial software tools the diffuse component is usually attributed to the internal surfaces in simple ways, without accounting for the sun position. For example, the commercial software TRNSYS distributes the diffuse radiation according to the absorptance-weighted area ratios of each surface. The distribution of the beam component on the internal surfaces of an enclosure has been modelled in various ways in the literature (see e.g. Chatziangelidis & Bouris [41], Kontoleon [42] and ASHRAE

Fundamentals [43]). In the present study, we consider the different absorptance values of the walls and the floor, and the fact that a fraction of the entering solar radiation re-escapes through the window after being reflected by the internal surfaces. For more details the reader can refer to Cattarin et al. [13].

The glazing is modelled by three thermal nodes, one for each glass pane. The thermo-optical behaviour of the transparent test sample is described considering the dependency of the glazing properties on the angle of incidence of beam solar radiation, while the behaviour of the test sample under diffuse radiation is treated, as suggested by Duffie and Beckman [40] and Davies [2], considering an *equivalent angle of incidence* of 60°. The angular-dependent optical properties of the glazing system are calculated using the software tool WINDOW v7.4.8.0 by Berkeley Lab. The library of the software already contains the optical properties of the commercial panes used in the window (low-emissivity coatings on faces 2 and 5, argon-filled (90%) gaps). The frame has not been modelled separately; the correspondent front area has been treated as if it were occupied by the support wall..

The model is integrated using the ODE15i implicit solver provided by Matlab and set to provide results every minute (corresponding to the time step of the measurements). The simulation over the considered period took approximately 13 minutes to complete.

4. Results of the thermal simulation

The internal and external temperature profiles of the north, east and west walls are reported in Figure 3.a. The measured values are represented with the respective uncertainty band (± 0.4 °C). The temperature residuals (calculated as *simulated value minus measured value at the same time t*) for the internal air and the internal and external surfaces of the envelope are reported in Figure 3.b. The residuals lie within a ±1 °C interval, usually lying within the measurement uncertainty bands (± 0.4 °C). They are higher (in absolute value) in days with high levels of solar radiation and a large ratio beam/global and show a systematic daily variation. In Figure 3.c the total diffuse radiation (including sky-diffused and ground-reflected) and the beam solar radiation on the south façade is depicted. Finally, Figure 3.d reports the external air temperature and the average temperature of the air in the guard zone close to the external surfaces of the test cell's walls; a

boundary condition of the Robin type is used to connect our model with the measured air temperature of the guard zone.

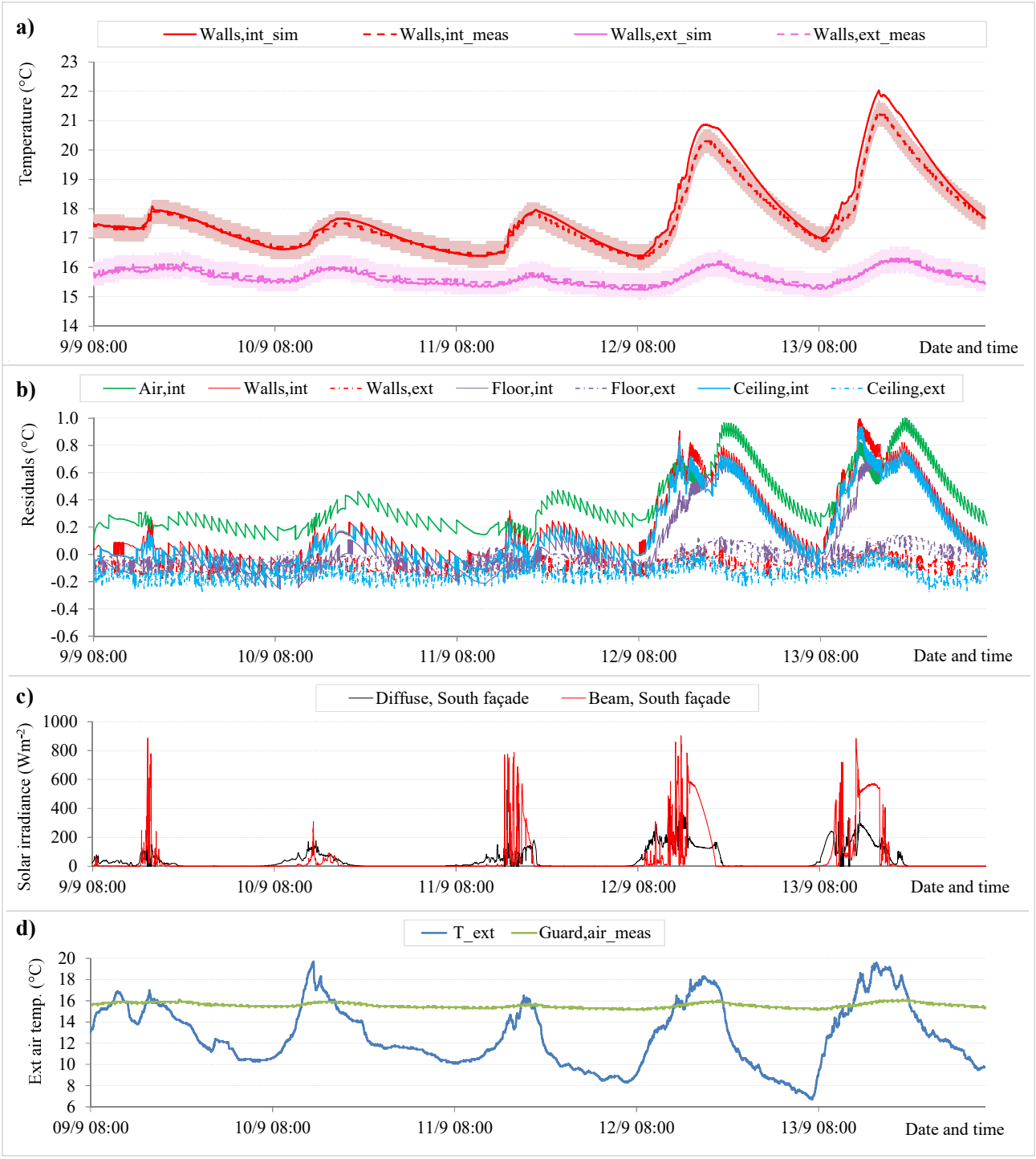

Figure 3. From top to bottom: a) simulated (*sim*) and measured (*meas*) temperatures of the internal and external surfaces of the north, east and west walls. b) profiles of residuals (*calculated minus measured*). c) total diffuse and beam solar radiation on the south façade. d) external air temperature and air temperature in the guard zone.

5. Local sensitivity analysis

This section presents the methodology and the results of a local sensitivity analysis applied to our thermal model, which highlights the parameters and inputs that are particularly influential (*sensitive*) on the temperature evolution of the test cell. In particular, we chose as model outputs the temperatures of the internal air, of the internal surfaces of the walls, of the test sample, of the floor and the ceiling. The aim is to identify the most sensitive parameters, which should therefore receive the utmost consideration both by the modeller and by the team performing the experimental campaign, and should be measured or estimated with the highest possible accuracy.

5.1. Methodology

As reported in Session 1.3, sensitivity analysis techniques are classified in local and global methods. Local sensitivity analysis (also called differential sensitivity analysis) methods allow to identify the set of most significant input parameters in terms of influence on the output variability by applying one-at-a-time variations around the parameters' nominal values; on the other hand they explore only a reduced space around a base case [22]. Global sensitivity analysis methods, by evaluating the interactions between parameters, extend the analysis to the whole input space. Considering that in our case (the analysis of an existing test cell rather than the design of a new one) some of the parameters have a limited variability/uncertainty, we limited ourselves to a local analysis around the base case. This might be able to capture a relatively large fraction of the total variance of outputs. For example Ruiz et al. [44] by performing a global sensitivity analysis of a office building in six climates (within IEA Annex 53 "Total Energy Use in Buildings: Analysis and evaluation methods") found that first order effects were accounting for more than 90% of the total variance of outputs. As observed by Tian: "The local sensitivity analysis is the simplest method and still very useful in building performance analysis even with its shortcomings. This is due to its low computational cost, simple implementation, and easy interpretation" [22]. In case the objective would be the design of a new facility, where most parameters may still be subject to the choice of the research team, including room dimensions and material properties, a global approach would be preferable.

In the following analysis we choose 49 parameters (such as material properties) and inputs (such as boundary conditions) and we apply a perturbation of + 5% to their nominal value. The simulation with nominal values

of the parameters/inputs is taken as a reference (base case), while each simulation run is compared to the base case using sensitivity indices proportional to the partial derivatives of the output y_i with respect to the chosen input parameter x_i. Various methods exist to compute the partial derivatives, such as the finite-difference method, the direct method, the Green functions and the method by Miller and Frenklac [45]. We use the finite-difference method, which is the most straightforward to implement. We use the sensitivity indices $S_i^*(t)$ in order to have the same unit of measurement of the output variables (°C), as done by Spitz et al. [29] and Bontemps [45], and we calculate them at each time step t. The first forward difference of $y(x_i)$ is used for the numerical approximation

$$S_i^*(t) = x_{i,0} \frac{y(x_i + \Delta x_i) - y(x_i)}{\Delta x_i} \tag{2}$$

where Δx_i is the variation (perturbation) of the input parameter. As reported by Kavgic et al. [46], the choice of Δx_i affects the accuracy of the computed sensitivities, as too large values may compromise the assumption of local linearity whilst a too small variation can result in high round-off errors. In the present case we set Δx_i equal to + 5% of the nominal value, consistently with the work by Bontemps [45].

Spitz et al. [29] state that sensitivity analysis can be applied only to constant parameters, since it is impossible to calculate the sensitivity index of parameters that vary during the simulation. However, as observed by Klepper [47], it is usually possible to reformulate inputs and initial conditions in terms of parameters. We decided to extend the definition of the sensitivity index to model inputs (such as solar radiation and external air temperature), considering as nominal value the actual nominal time series $x_{i,0}(t)$, that is the time series of monitored data. These inputs are varied at each time step by a fixed quantity (+1°C in the case of temperatures) or as a percentage of the nominal value (+5% in the case of solar radiation). In this way, it is possible to evaluate also the model inputs and answer the question of which measurements are more critical and should therefore be taken with the highest possible accuracy. As suggested in Spitz et al. [29] and Bontemps [49], we calculate the *distance* of each sensitivity index as:

$$S_{i,d}^* = \sqrt{\left(S_{i,m}^*\right)^2 + \left(S_{i,std}^*\right)^2} \tag{3}$$

where $S_{i,m}^{*}$ and $S_{i,std}^{*}$ are the mean and the standard deviation of S_i^{*} over the considered period. Distances are useful to detect indices that have a low mean value but a high variation, as pointed out by Spitz et al. [29].

In order to reduce the computation time, before running the simulations we resample the data as hourly values. The sensitivity indices are calculated for five model outputs, that is the temperatures of: (i) the internal air (*T air,int*), (ii) the internal surfaces of the walls (*T walls,int*), (iii) the internal glass pane of the test sample (*T test,int*), (iv) the internal surfaces of the floor (*T floor,int*) and (v) the ceiling (*T ceiling,int*).

5.2. Results and discussion

As it can be observed in Figure 4, twelve sensitivity indices (calculated as from Eq. 3) present a distance higher than 0.5 °C, those related to the following parameters and inputs:

- the air temperature in the guard zone,
- the initial temperature(s) of the test cell envelope,
- the linear dimension of the square window,
- the solar irradiance on the vertical plane of the window,
- the depth of the test cell,
- the thermal conductivity of the polyurethane layer in the envelope,
- the thickness of the polyurethane layer in the envelope,
- the solar direct transmittance of the glazing,
- the internal height of the test cell,
- the internal width of the test cell,
- the external air temperature,
- the electrical power input to the mixing fan.

The complete bar diagram for the analysed parameters is reported in Figure 4 (top), while Figure 4 (bottom) shows the temporal evolution of the distances of the sensitivity indices corresponding to the twelve most *sensitive* parameters. Several considerations can be drawn from Figure 4:

1. The initial temperatures of the envelope have by far the greatest influence during the first simulated day, while their impact decreases down to negligible values after a couple of days.

2. On the contrary, the air temperature in the guard zone has little impact in the first hours of simulation (since the thermal wave generated by a potential temperature difference between the guard zone and the interior of the test cell takes time to penetrate through the envelope), while it becomes the most *sensitive* variable in the following days of the simulation. The importance of the air temperature in the guard zone derives by the fact that the test cell is surrounded by the guard zone on five sides, that is on about 88% of the surface area of the test cell envelope.
3. The parameters related to the window (*edge_glz_WIN*, τ_90_WIN, *tilt_angle_WIN*, see Table 5 for their meanings) and the solar irradiance on a vertical plane (*Gv*, model input) become more *sensitive* under clear(er) sky conditions (i.e., the last two simulated days).
4. The internal dimensions of the test cell and the thermal properties of its insulation layers play a key role in the thermal dynamics, being involved both in the transmission heat transfer coefficient of the envelope (via the surface areas) and in the thermal capacity of the system (via the volume of the envelope).
5. For simplicity, the distances of sensitivity indices in Figure 4 are ranked based on the average value obtained for the five analysed model outputs. However, in some cases the ranking of the variables based on the distances of the sensitivity indices depends on the specific model output. For example the model output *T test,int* is relatively more sensitive to the input *T ext* than to the other input parameters. The obvious physical explanation is that the internal window pane is, compared to the other internal surfaces of the test cell, more influenced by the external temperature because it is separated from the external environment only by the other two glass panes.

The consideration at point 4 is also linked to the specific experimental conditions: in free-running mode the envelope experiences large temperature variations under the external stimuli of solar radiation and external air temperature. If the test cell were kept at a fixed set-point temperature (the same of the guard zone), then some of the model inputs (such as the temperature in the guard zone) and model parameters (such as the thermal conductivity of the polyurethane, its volumetric heat capacity or the internal dimensions of the test cell) would play a less significant role. In addition, if we limit the calculation of the distances $S^*_{i,d}$ to the last, fairly sunny day (13th September), the solar direct transmittance and the tilt angle of the window become more important than considering the average over the entire period. Therefore, care should be taken when interpreting the results that depend on the operating strategy and conditions.

Finally, a certain number of parameters and inputs may be considered *insensitive*, for example: (i) the thermal emissivity of the internal surfaces, (ii) the thermal conductivity values of the steel sheets, the glass panes, the external cladding and the wooden flooring, (iii) the view factors to the sky and the surroundings, (iv) the sky-dome temperature, and others. However, care should be taken when interpreting these results. These parameters can be considered insensitive only for the range of conditions under which the thermal model has been validated. For example, the presented model does not treat hygrothermal phenomena; therefore, on rainy days and if the building envelope were constituted by highly hygroscopic materials, using our modelling approach would lead to higher residuals on the internal temperatures, due to the variation of the thermal conductivity with the water content. In order to better predict the thermal dynamics of the test cell on rainy/snowy days, the algorithms should be expanded to treat hygrothermal phenomena, validated and subjected to a new sensitivity analysis, possibly including other model parameters and inputs.

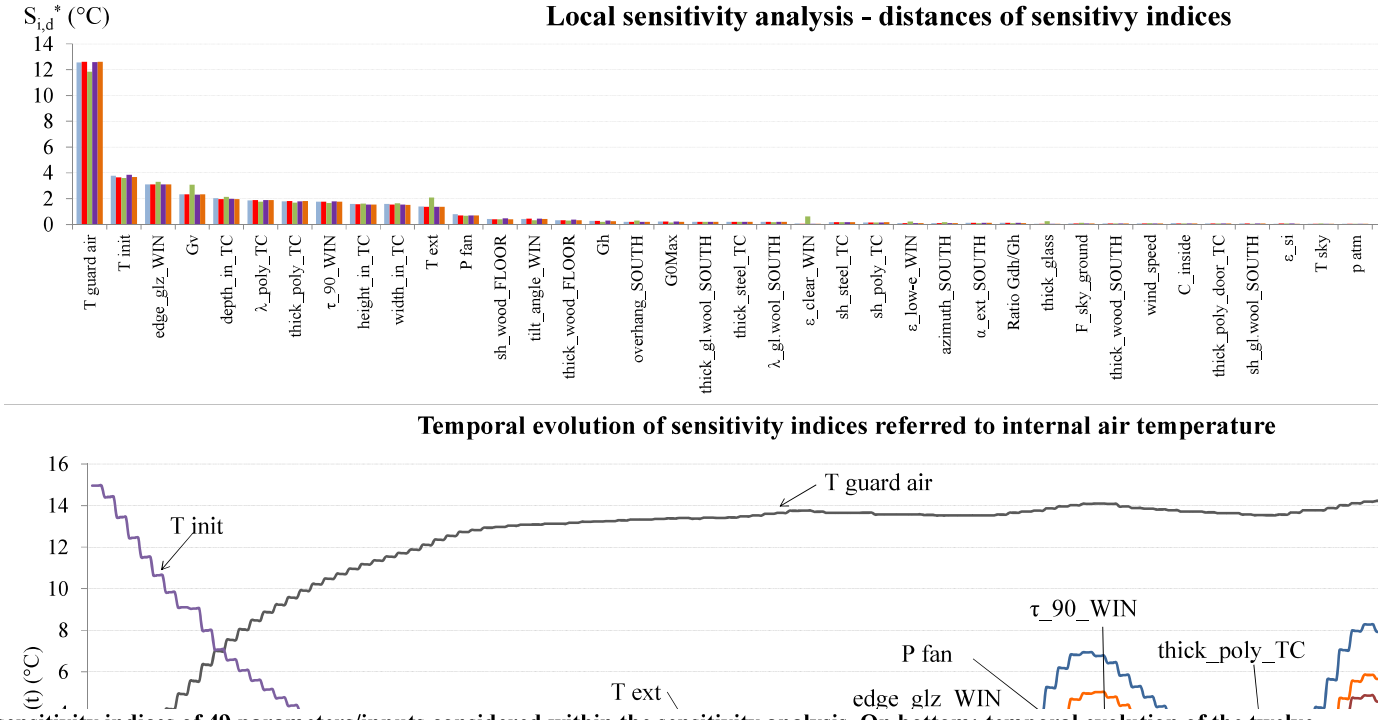

Figure 4. On top: distances of the sensitivity indices of 49 parameters/inputs considered within the sensitivity analysis. On bottom: temporal evolution of the twelve distances calculated for the most sensitive parameters/inputs and calculated with reference to the internal-air temperature. The meanings of the variables' names are reported in Table 5.

Table 5. Model parameters and inputs studied within the sensitivity analysis (in alphabetic order)

Parameter / input	Unit of measurement
azimuth_SOUTH: surface azimuth of south wall	(°)
C_inside: internal thermal capacity	(J K^{-1})
depth_in_TC: internal depth of test cell	(m)
edge_glz_WIN: linear dimension of (square) window	(m)
F_sky_ground: view factors to the sky and the ground/surroundings	(-)
G0Max: solar constant	(W m^{-2})
Gh: global solar irradiance on a horizontal plane	(W m^{-2})
Gv: global solar irradiance on a south-oriented vertical plane (same orientation of test sample)	(W m^{-2})
height_door_TC: height of the door	(m)
height_in_TC: internal height of the test cell	(m)
overhang_SOUTH: overhang of south wall with respect to the external glass pane	(m)
p atm: atmospheric pressure	(hPa)
P fan: electrical power consumption due to mixing fan	(W)
Ratio Gdh/Gh: ratio between diffuse and global irradiance on the horizontal plane	(-)
RH ext: external relative humidity (used in the calculation of the sky temperature)	(%)
sh_clad_SOUTH: volumetric heat capacity of cladding, south wall	(J.$m^{-3}K^{-1}$)
sh_gl.wool_SOUTH: volumetric heat capacity of glass wool	(J m^{-3} K^{-1})
sh_poly_TC: volumetric heat capacity of polyurethane	(J m^{-3} K^{-1})
sh_steel_TC: volumetric heat capacity of steel	(J m^{-3} K^{-1})
sh_wood_FLOOR: volumetric heat capacity of floor slab	(J m^{-3} K^{-1})
T ext: external air temperature	(°C)
T guard air: air temperature in the guard zone	(°C)
T init: initial temperatures of the envelope	(°C)
T sky: sky temperature, estimated according to the model by Martin [48]	(°C)
thick_clad_SOUTH: thickness of cladding, south wall	(m)
thick_gl.wool_SOUTH: thickness of glass wool, south wall	(m)
thick_glass: thickness of glass panes	(m)
thick_poly_door_TC: thickness of polyurethane, door	(m)
thick_poly_TC: thickness of polyurethane layer (walls, floor and ceiling slabs)	(m)
thick_steel_TC: thickness of steel, envelope	(m)
thick_wood_FLOOR: thickness of wooden panel, floor	(m)
thick_wood_SOUTH: thickness of wooden panel, south wall	(m)
tilt_angle_WIN: tilt angle of the window	(m)
width_door_TC: width of the door	(m)
width_in_TC: internal width of the test cell	(m)
α_ext_SOUTH: external absorptance of the south wall	(-)
α_int_FLOOR: absorptance, floor surface	(-)
α_int_walls_TC: absorptance, internal surfaces	(-)
ε_clear_WIN: hemispherical emissivity of clear-glass panes	(-)
ε_low-e_WIN: hemispherical emissivity of low-emissivity pane	(-)

ε_si: hemispherical emissivity of internal surfaces	(-)
λ_clad_SOUTH: thermal conductivity of cladding, south wall	(W $m^{-1}K^{-1}$)
λ_gl.wool_SOUTH: thermal conductivity of glass wool, south wall	(W m^{-1} K^{-1})
λ_glass_WIN: thermal conductivity of glass, window	(W $m^{-1}K^{-1}$)
λ_poly_TC: thermal conductivity of polyurethane	(W m^{-1} K^{-1})
λ_steel_TC: thermal conductivity of steel, envelope	(W $m^{-1}K^{-1}$)
λ_wood_FLOOR: thermal conductivity of wooden flooring	(W $m^{-1}K^{-1}$)
τ_90_WIN: solar direct transmittance of the window	(-)

6. Conclusions

The paper presents the methodology and the main results of the validation of a lumped-parameter thermal model of the ZEB Test Cells Laboratory, located in the Gløshaugen campus of NTNU and SINTEF in Trondheim, Norway. A dedicated experimental campaign provided the *benchmark* for the experimental validation of the developed thermal model. The results of the validation show that the model is generally able to predict the thermal dynamics of the test cell, with residuals lying within a ±1 °C interval and lying, most of the time, within the measurement uncertainty bands (± 0.4 °C). The residuals show a systematic daily variation and are higher in sunny days, suggesting that the discrepancies may be attributed to the window's optical properties and/or to the modelling of the impinging solar radiation.

We performed a local sensitivity analysis in order to identify the model parameters and inputs that have the highest influence on the calculation of chosen model outputs (here, the temperature of the internal air and of some internal surfaces). The analysis shows that, under the presented free-running scenario, the most important parameters and inputs out of the 49 tested ones are: the air temperature in the guard zone, the initial temperature(s) of the test cell envelope, the linear dimension of the square window, the solar irradiance on the vertical plane of the window, the depth of the test cell, the thermal conductivity and the thickness of the polyurethane layer in the envelope, the solar direct transmittance of the glazing, the internal height and width of the test cell, the external air temperature and the electrical power input to the mixing fan.

Based on the local sensitivity analysis and on in-field observations, some actions are suggested in order to improve the quality of the input data provided to a simulation tool, and hence increase the accuracy of the predictions of the thermal behaviour of the test cell:

- running the test cell for at least a week, in order to reduce the influence of the initial conditions of the experimental facility. If possible, it would be beneficial to start the test cell from a well-known thermal state. This could be done by shielding and conditioning the wall exposed to the exterior by means of an external conditioning box and by running the guard zone at constant temperature set-point for at least three days;
- monitoring accurately the environmental conditions in the guard zone (e.g., calibrate all temperature sensors regularly, cover the external surfaces of the test cell with low-emissivity foils in order to minimize their radiative heat exchanges with the internal surfaces of the guard zone. This would in turn minimize the influence of the mean radiant temperature of the guard zone *seen* by the external surfaces, which could be non-uniform and hence rather challenging to measure). The accurate monitoring of the environmental conditions in the guard zone is of particular concern when the test cell is in free-running mode, while it becomes less relevant when the guard zone and the test cell are actively maintained at the same set-point temperature (Section 5.2);
- if the goal of the experiment is the validation of a thermal model of the test cell (and not the characterization of a transparent test sample), checking that the thermo-optical properties of the installed transparent component are accurately known, since the entering solar load is one of the main drivers of the test cell's thermal dynamics;
- measuring accurately the internal dimensions of the test cell, which are involved both in the transmission heat transfer coefficient of the envelope (via the surface areas) and in the thermal capacity of the system (via the volume of the envelope);
- measuring the thermal conductivity of the insulation layers (e.g., by means of a hot plate apparatus);
- installing a global irradiance pyranometer on the same vertical plane and next to the window, in order to reduce the uncertainty related to the entering solar load. If possible, install a sun-tracking pyrheliometer in order to accurately measure the beam normal radiation;

The influence of a model parameter depends also on the specific experimental conditions and on the algorithms used by the thermal model. Thermal simulations and local sensitivity analyses applied to a range of expected operating conditions can guide the design process of new test cell facilities, highlighting the most critical measurements and supporting the research team in the choice of the features of the envelope, of

the conditioning system and of the measurement set-up. For the design of a new facility, however, the use of a global sensitivity analysis is recommended in order to include the effect of potential design parameter interactions by exploring the whole input space.

Acknowledgements

The activities presented in this paper have been partially carried out in the framework of the Research Project 255252/E20, financed by the Research Council of Norway and the industrial partners Saint-Gobain Byggevarer AS, NorDan AS, and Schuco International KG, and in the framework of the research activities in the EU Cost Action TU1403 “Adaptive Facades Network”. Financial support for the Short Term Scientific Mission of PhD candidate Giulio Cattarin was provided by the EU Cost Action TU1403 “Adaptive Facades Network”.

References

[1] A. Athienitis et M. Santamouris, Thermal Analysis and Design of Passive Solar Buildings, New York: Routledge, 2002.

[2] M. G. Davies, Building Heat Transfer, Wiley, 2004.

[3] C. Underwood et F. Yik, Modelling Methods for Energy in Buildings, Blackwell, 2004.

[4] G. Hudson and C. P. Underwood, “A simple building modelling procedure for Matlab/Simulink,” 1999.

[5] K. A. Antonopoulos et E. Koronaki, «Envelope and indoor thermal capacitance of buildings,» *Applied Thermal Engineering,* vol. 19, pp. 743-756, 1999.

[6] K. Lee et J. E. Braun, «Model-based demand-limiting control of building thermal mass,» *Building and Environment,* vol. 43, p. 1633–1646, 2008.

[7] M. M. Gouda, S. Danaher and C. Underwood, “Building thermal model reduction using nonlinear constrained optimization,” *Building and Environment,* vol. 37, pp. 1255-1265, 2002.

[8] G. Fraisse, C. Viardot, O. Lafabrie et G. Achard, «Development of a simplified and accurate building model based on electrical analogy,» *Energy and Buildings,* vol. 34, pp. 1017-1031, 2002.

[9] C. P. Underwood, “An improved lumped parameter method for building thermal modelling,” *Energy and Building,* vol. 79, pp. 191-201, 2014.

[10] T. Trucano, L. Swiler, T. Igusa, W. Oberkampf et M. Pilch, «Calibration, validation, and sensitivity analysis: What's what,» *Reliability Engineering and System Safety,* vol. 91, p. 1331–1357, 2006.

[11] R. Judkoff, D. Wortman et J. Burch, «Empirical Validation of Building Analysis Simulation Programs: A Status Report,» Solar Energy Research Institute, Colorado, 1982.

[12] R. Judkoff, D. Wortman, B. O'Doherty et J. Burch, «A methodology for validating building energy analysis simulations,» National Renewable Energy Laboratory, Golden, CO, 2008.

[13] G. Cattarin, L. Pagliano, F. Causone et A. Kindinis, «Empirical and comparative validation of an original model to simulate the thermal,» *Energy and Buildings (under final review),* 2017.

[14] G. Cattarin, F. Causone, A. Kindinis et L. Pagliano, «Outdoor test cells for building envelope experimental characterization – a literature review,» *Renewable and Sustainable Energy Reviews,* vol. 54, pp. 606-625, 2016.

[15] A. Saltelli, F. Tarantola, F. Campolongo et M. Ratto, Sensitivity Analysis in Practice: A Guide to Assessing Scientific Models, John Wiley & Sons Ltd., 2004.

[16] J. Lam et S. Hui, «Sensitivity Analysis of Energy Performance of Office Buildings,» *Bulding and Environment,* vol. 31, n° %11, pp. 27-39, 1996.

[17] H. Shen et A. Tzempelikos, «Sensitivity analysis on daylighting and energy performance of perimeter offices with automated shading,» *Building and Environment,* vol. 59, pp. 303-314, 2013.

[18] H. Breesch et A. Janssens, «Performance evaluation of passive cooling in office buildings based on uncertainty and sensitivity analysis,» *Solar Energy,* vol. 84, p. 1453–1467, 2010.

[19] L. Pagliano, G. Cattarin, F. Causone et A. Kindinis, «Improved methods for the calorimetric determination of the solar factor in outdoor test cell facilities,» *Energy and Buildings (In Press, Accepted Manuscript),* 2017.

[20] W. Tian, «A review of sensitivity analysis methods in building energy analysis,» *Renewable and Sustainable Energy Reviews,* vol. 20, p. 411–419, 2013.

[21] A. Irving, «Stochastic sensitivity analysis,» *Appl. Math. Modelling,* vol. 16, 1992.

[22] W. Tian et P. de Wilde, «Uncertainty and sensitivity analysis of building performance using probabilistic climate projections: A UK case study,» *Automation in Construction,* vol. 20, p. 1096–1109, 2011.

[23] P. Heiselberg, H. Brohus, A. Hesselholt, H. Rasmussen, E. Seinre et S. Thomas , «Application of sensitivity analysis in design of sustainable buildings,» *Renewable Energy,* vol. 34, p. 2030–2036, 2009.

[24] M. Kristensen et S. Petersen, «Choosing the appropriate sensitivity analysis method for building energy model-based investigations,» *Energy and Buildings,* vol. 130, p. 166–176, 2016.

[25] E. Borgonovo et E. Plischke, «Sensitivity analysis: A review of recent advances,» *European Journal of Operational Research,* vol. 248, p. 869–887, 2016.

[26] P. Ferreira Tavares et A. Gomes Martins, «Energy efficient building design using sensitivity analysis—A case study,» *Energy and Buildings,* vol. 39, p. 23–31, 2007.

[27] J. Lam, K. Wana et L. Yang, «Sensitivity analysis and energy conservation measures implications,» *Energy Conversion and Management,* vol. 49, p. 3170–3177, 2008.

[28] K. Goethals, H. Breesch et A. Janssens, «Sensitivity analysis of predicted night cooling performance to internal convective heat transfer modelling,» *Energy and Buildings,* vol. 43, p. 2429–2441, 2011.

[29] C. Spitz, L. Mora, E. Wurtz et A. Jay, «Practical application of uncertainty analysis and sensitivity analysis on an experimental house,» *Energy and Buildings,* vol. 55, p. 459–470, 2012.

[30] D. Sanchez, B. Lacarrière, M. Musy et B. Bourges, «Application of sensitivity analysis in building energy simulations: Combining first- and second-order elementary effects methods,» *Energy and Buildings,* vol. 68, p. 741–750, 2014.

[31] S. Yang, W. Tian, E. Cubi, Q. Meng, Y. Liu et L. Wei, «Comparison of Sensitivity Analysis Methods in Building Energy Assessment,» *Procedia Engineering,* vol. 146, p. 174 –181, 2016.

[32] F. Causone, M. Doya, F. Goia, O. Larsen , A. Kindinis et V. Serra, «Experimental facilities for adaptive façades characterization,» chez *10th Conference on Advanced Building Skins*, Bern, 2015.

[33] N. Mateus , A. Pinto et G. da Graça, «Validation of EnergyPlus thermal simulation of a double skin naturally and mechanically ventilated test cell,» *Energy and Buildings,* vol. 75, p. 511–522, 2014.

[34] B. Slosharek, «ZEB Test Cells - Thermal bridge calculations (Internal report),» ZEB - Research centre on Zero Emission Buildings, Trondheim, 2015.

[35] A. Khalifa et R. Marshall, «Validation of heat transfer coefficients on interior building surfaces using a real-sized indoor test cell,» *Int. J. Heat Mass Transfer,* vol. 33, pp. 2219-2236, 1990.

[36] A. Hatton et H. Awbi, «Convective heat transfer in rooms,» chez *Building Simulation '95, Fourth International Conference Proceedings*, Madison, USA, 1995.

[37] W. Rohsenow, J. Hartnett et Y. Cho, Handbook of Heat Transfer - 3rd Edition, McGraw-Hill éd., 1998.

[38] D. Reindl, W. Beckman et J. Duffie, «Diffuse Fraction Correlations,» *Solar Energy 45 (1),* pp. 1-7, 1990.

[39] TRNSYS 17, *TRNSYS 17 documentation. A Transient System Simulation Programme Volume 4 - Mathematical Reference.*

[40] J. Duffie et W. Beckman, Solar Engineering of Thermal Processes, New York: John Wiley & Sons Inc, 1991.

[41] K. Chatziangelidis et D. Bouris, «Calculation of the distribution of incoming solar radiation in enclosures,» *Applied Thermal Engineering,* vol. 29, p. 1096–1105, 2009.

[42] K. Kontoleon, «Dynamic thermal circuit modelling with distribution of internal solar radiation on

varying fac¸ade orientations,» *Energy and Buildings,* vol. 47, pp. 139-150, 2012.

[43] ASHRAE, Fundamental Handbook, ASHRAE, 2009.

[44] R. Ruiz, S. Bertagnolio et V. Lemor, «Global Sensitivity Analysis applied to Total Energy Use in Buildings,» chez *International High Performance Buildings Conference*, Purdue, 2012.

[45] S. Bontemps, «Validation expérimentale de modèles : application aux bâtiments basse consommation (in French),» Université de Bordeaux, 2015.

[46] M. Kavgic , D. Mumovic , A. Summerfield, Z. Stevanovic et O. Ecim-Djuric, «Uncertainty and modeling energy consumption: Sensitivity analysis for a city-scale domestic energy model,» *Energy and Buildings,* vol. 60, p. 1–11, 2013.

[47] O. Klepper, «Multivariate aspects of model uncertainty analysis: tools for sensitivity analysis and calibration,» *Ecological Modelling,* vol. 101, pp. 1-13, 1997.

[48] M. Martin et P. Berdahl, «Characteristics of Infrared Sky Radiation in the United States,» *Solar Energy,* vol. 33, n° %13/4, pp. 321-336, 1984.